Bi-substitution-induced magnetic moment distribution in spinel $Bi_xCo_{2-x}MnO_4$ multiferroic

N E Rajeevan[1], Ravi Kumar[2,7], D K Shukla[3], P Thakur[4], N B Brookes[4], K H Chae[5], W K Choi[5], S Gautam[5], S K Arora[6], I V Shvets[6] and P P Pradyumnan[1]

[1] Department of Physics, University of Calicut, Kerala 673635, India
[2] Materials Science Division, Inter University Accelerator Centre, Aruna Asaf Ali Marg, New Delhi 110067, India
[3] Department of Physics, Aligarh Muslim University, Aligarh 202002, India
[4] European Synchrotron Radiation Facility, BP 220, F-38043 Grenoble Cedex, France
[5] Materials Science and Technology Research Division, KIST, Seoul 136791, Korea
[6] CRANN, School of Physics, Trinity College Dublin, Dublin 2, Republic of Ireland

Abstract

We report the near-edge x-ray absorption spectroscopy (NEXAFS) at the Co/Mn $L_{3,2}$ edge and oxygen K edge of the well-characterized Bi-substituted Co_2MnO_4 multiferroic samples. The evolution of peak features in NEXAFS spectra of the Co/Mn $L_{3,2}$ edge and O K edge show the Bi-induced redistribution of magnetic cations (Co/Mn). The variation in valence states of Co and Mn in all the substituted compositions is consistent with the observed ferrimagnetic behaviour of the samples. Magnetization data show the decrease in molecular f eld complementing the ferrimagnetism. The role of Bi in the enhancement of magnetic interactions as well as the appearance of ferroelectricity in $Bi_xCo_{2-x}MnO_4$ ($0 \leqslant x \leqslant 0.3$) is discussed.

1. Introduction

Multiferroics (MF) are the materials that enfold physics for various future technological applications and have received worldwide attention from the scientif c community working in the f eld of materials sciences [1, 2]. Coexisting magnetism and ferroelectricity along with coupling between them ensures the possibility of technological uses for these materials but it is hard to achieve the above order parameters in a single phase due to their contrasting origins. Various alternative mechanisms have been proposed as a solution to this problem, including an approach to achieving the ferromagnetism with non-metallicity or ferroelectricity in centrosymmetric systems [3, 4]. These materials are time-honoured systems owing to their extraordinary magnetic and electric properties, which appeared as the source of the most fascinating tunable magnetoelectric behaviour, by changing the chemical composition and cation redistribution [4–11].

The crystal symmetry in spinel oxides offers ample opportunities for testing/designing new functional properties with numerous permutations and combinations possible at A and B sites. The charge distribution of the normal spinel is represented by $[A^{2+}]_{8a}[B_2^{3+}]_{16d}[O_4^{2-}]_{32e}$, in which Wyckoff positions 8a denote the tetrahedral sites and 16d the octahedral sites surrounded by O^{2-} ions at 32e sites. Empty interstitial space is comprised of 16 octahedral sites (16c) and 56 tetrahedral sites (8b and 48f). In the Co-based spinel oxides the substituted trivalent metal ion occupies the octahedral sites, while cobalt ions are distributed over both octahedral (Co^{3+} ions in low spin $t_{2g}^6e_g^0$ state) and tetrahedral sites (magnetic Co^{2+} ions in high spin $e_g^4t_{2g}^3$ state) [12]. Recently we have reported the magnetoelectric multiferroic properties of Bi-substituted Co_2MnO_4, which crystallizes into

[7] Author to whom any correspondence should be addressed.

a normal spinel with O_h^7-$Fd\bar{3}m$ space group [13, 14]. In $Bi_xCo_{2-x}MnO_4$, Bi^{3+} with $6s^2$ lone pair electrons at the octahedral sites instead of magnetic ions, distorts the oxygen octahedron and consequently introduces ferroelectricity and inf uences the ferrimagnetic ordering of the parent system. Mixed valence states of this spinel oxide plays a key role in determining the electrical and magnetic characteristics and requires further investigations to understand the intriguing nature of spin state distribution and hybridization states. The deeper understanding of the electronic structure of these spinel oxides would be desirable to design new MF materials and understand their complex magnetic ordering, which has a profound effect on ferroelectric behaviour. It necessitates the use of powerful microscopic experimental tools like near-edge x-ray absorption f ne structure (NEXAFS) and extended x-ray absorption f ne structure (EXAFS). Owing to its simplicity and universality, the NEXAFS technique is most widely used in determining the valence states of atoms and local site symmetries in solids. Here, we report the electronic structure of multiferroic-magnetoelectric $Bi_xCo_{2-x}MnO_4$ ($0 \leqslant x \leqslant 0.3$) samples using x-ray absorption spectroscopy (XAS). In this study, the NEXAFS spectra at the O K, Mn $L_{3,2}$ and Co $L_{3,2}$ edges of $Bi_xCo_{2-x}MnO_4$ ($0 \leqslant x \leqslant 0.3$) along with the reference compounds Bi_2O_3, CoO, $LiCoO_2$, MnO and MnO_2 are presented. Magnetization results are correlated to the cation distribution.

2. Experimental details

Polycrystalline single-phase $Bi_xCo_{2-x}MnO_4$ ($0.0 \leqslant x \leqslant 0.3$) samples were synthesized by the standard solid state reaction technique. The details of materials synthesis together with structural, magnetic, ferroelectric and coupling studies are presented elsewhere [13, 14]. The NEXAFS measurements of $Bi_xCo_{2-x}MnO_4$ ($0.0 \leqslant x \leqslant 0.3$) along with Co_3O_4, CoO, MnO, MnO_2, and Bi_2O_3 at O K, Co $L_{3,2}$ and Mn $L_{3,2}$ edges were performed at the soft x-ray beamline 7B1 XAS KIST of the Pohang Light Source and some parts of the measurements were repeated at the ESRF's ID08 beamline, which uses an APPLE II type undulator giving ∼100% linear/circular polarization. All the samples were scraped with diamond foil prior to the measurements in order to remove the surface contaminants. The spectra were collected simultaneously in both total electron yield (TEY) and total f uorescence yield (TFY) modes at room temperature, ensuring both surface and bulk sensitivities. The spectra were normalized to incident photon f ux and the base pressure of the experimental chamber was better than 5×10^{-10} Torr. The Raman spectra were recorded at room temperature in backscattering conf guration using a HR800 Jobin-Yvon spectrometer having a resolution of 1 cm^{-1}. An He–Ne laser (488 nm) was used as an excitation source at 9 mW power. Magnetization measurements were performed using the vibrating sample magnetometer (VSM) option of the Quantum Design (PPMS) set-up.

3. Results and discussions

Spinel oxides exhibit a variety of exciting physical properties due to the active role of the orbital degrees of freedom within its complicated structure, which can be typically observed in the lattice and electronic response. As a matter of fact, such properties appear to have their origin in the unique electronic structure derived from the hybridized transition metal ions' (TMI) 3d and O 2p orbitals in the structural and chemical environment of a spinel oxide [15]. It is reported that the substitution of Bi^{3+} (non-magnetic) ion with $6s^2$ lone pair introduces the non-centrosymmetric charge ordering, leading to ferroelectricity in Co_2MnO_4 simultaneously increasing the net magnetic moment [13, 14]. This can be attributed to the hybridization effects of Mn/Co 3d–O 2p orbitals with Bi 6sp orbitals. Possibly due to the larger ionic radii of Bi^{3+}, which may cause the redistribution of cations among the occupied 8a (tetrahedral-T_D) and 16d (octahedral-O_H) sites, and the participation of unoccupied 16 octahedral sites (16c) and 56 tetrahedral sites (8b and 48f) in a distorted environment due to Bi-induced chemical pressure.

NEXAFS spectra were assessed at the Mn/Co $L_{3,2}$ and O K edges for $Bi_xCo_{2-x}MnO_4$ ($x = 0.0$, 0.1, 0.2 and 0.3) samples. The Mn/Co $L_{3,2}$ edges directly proves the unoccupied Mn/Co 3d states via $2p \rightarrow 3d$ transitions, whereas the O K edges establish the unoccupied O 2p states via $O\ 1s \rightarrow 2p$ dipolar transitions [16], together providing the information on the Mn/Co 3d occupancy and the effect of Bi^{3+} ion substitution on the hybridization between the O 2p and Mn/Co 3d orbitals. It is well known that the peak positions and the spectral shapes of the Co/Mn $L_{3,2}$ edge NEXAFS spectrum depend on the local electronic structure of Co/Mn ions, and are sensitive to the crystal f eld symmetry due to the 2p–3d transitions. So the L edge spectrum provides information on the valence state of the Co/Mn ions [17, 18]. Figure 1 shows the normalized Co $L_{3,2}$ edge NEXAFS spectra of $Bi_xCo_{2-x}MnO_4$ ($0.0 \leqslant x \leqslant 0.3$) samples. The spin–orbit interaction of the Co 2p core states splits the spectrum into two broad multiplets, namely the L_3 ($2p_{3/2}$) and L_2 ($2p_{1/2}$) ∼15 eV apart. Each of these two regions further splits into t_{2g} and e_g orbital features because of the crystal f eld effect of neighbouring ions. The intensity of these peaks is the direct measure of total unoccupied Co 3d states. In Co_2MnO_4, the Co ions distributed at A and B sites (in the AB_2O_4 structure) are in T_D (Co^{2+}) and O_H (Co^{3+}) symmetries. Co^{3+} at the B (O_H) site has the higher crystal f eld splitting energy, so all the valence electrons are in a lower orbital t_{2g} ($t_{2g}^6 e_g^0$) only. In tetrahedral symmetry, the situation is reversed; the e_g subbands lie at lower energy than that of t_{2g}. The associated lower crystal f eld splitting energy results in the high spin state of Co^{2+} ($e_g^4 t_{2g}^3$). The L_3 region contains two spectral features, A_1 and B_1, at 775.8 eV and 777.2 eV, which correspond to Co^{2+} and Co^{3+} valence state, respectively. To determine the valence states of Co ions in $Bi_xCo_{2-x}MnO_4$, Co $L_{3,2}$ edges have been compared with those of CoO and $LiCoO_2$ spectra. For the starting composition Co_2MnO_4 ($x = 0.0$), the intensity ratio B_1/A_1 is almost equal to one, indicating that distribution of Co^{2+} ions at T_D and Co^{3+} ions at O_H, respectively, are equal. The B_1/A_1 ratio is found to increase with increase in Bi substitution, clearly showing that Co^{2+} content is reduced. This reveals that substitution of Bi at O_H sites enforces the relocation of Mn ions between O_H and T_D sites.

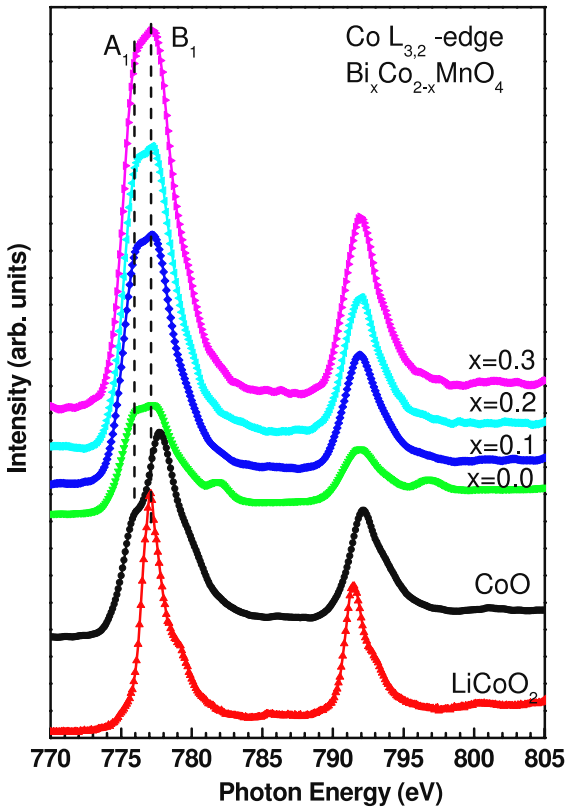

Figure 1. Normalized Co $L_{3,2}$ spectra of $Bi_xCo_{2-x}MnO_4$ ($x = 0.0$, 0.1, 0.2 and 0.3) along with the spectra of CoO and $LiCoO_2$.

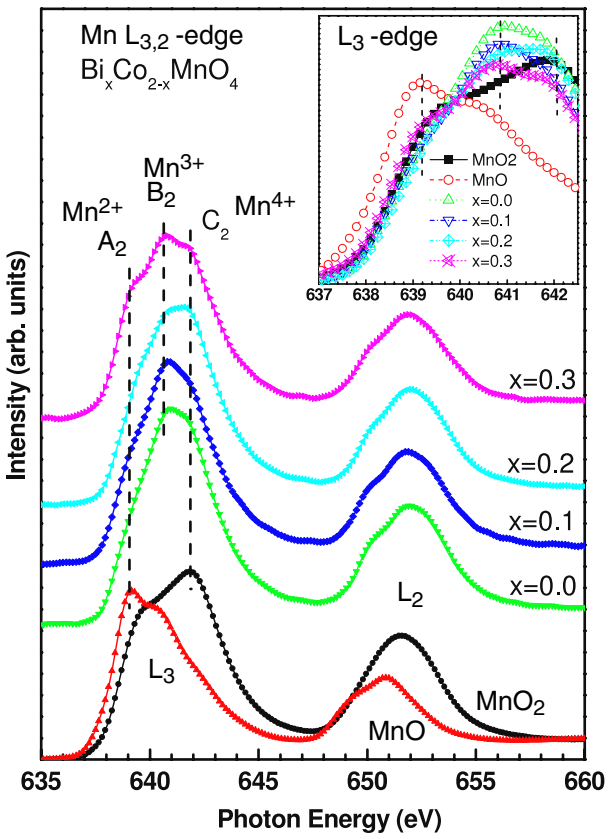

Figure 2. Normalized Mn $L_{3,2}$ spectra of $Bi_xCo_{2-x}MnO_4$ ($x = 0.0$, 0.1, 0.2 and 0.3) along with the spectra of MnO and MnO_2. Inset: zoomed-normalized Mn L_3-edge region.

Figure 2 shows the Mn $L_{3,2}$ spectra of $Bi_xCo_{2-x}MnO_4$ along with the reference compounds MnO and MnO_2. Similar to Co $L_{3,2}$ edge spectra (f gure 1) due to the spin–orbit interaction, Mn 2p core states split the spectrum into two broad multiplets, namely the L_3 ($2p_{3/2}$) and L_2 ($2p_{1/2}$) ∼11 eV apart. Each of these two regions further splits into t_{2g} and e_g orbital features because of the crystal fie d effect among the neighbouring ions. The intensity of these peaks measures the total unoccupied Mn 3d states. These spectra show a valence-specif c multiplet structure with a chemical shift due to changes in oxidation state. The inf ection points of the Mn L_3 edge for manganese oxides ($Mn^{2+}O$ and $Mn^{4+}O_2$ shown in the plot and $Mn_2^{3+}O_3$ from [19–21]) are subsequently at higher energies, corresponding to the increasing valence states of Mn. The L_3 region in both MnO_2 and MnO contains two spectral features, which are assigned to Mn t_{2g} and Mn e_g subbands. Mn ions in MnO have a 2+ valence state with orbitals each fi led by majority spin electrons, so that the feature at lower energy can be attributed to t_{2g} and the higher energy feature is attributed to e_g subbands. The larger intensity of the lower energy peak is due to the fact that there are three t_{2g} orbitals and only two e_g orbitals and t_{2g} have more unoccupied states. In MnO_2, Mn ions have a 4+ oxidation state with the e_g subband empty. So the unoccupied part of the e_g subband will contribute to the higher energy peak of the Mn $L_{3,2}$-edge spectrum, and is more intense. Similarly, in the case of Mn_2O_3 the L_3 edge is also dominated by e_g subbands only [19–21]. The L_3 region in Mn $L_{3,2}$ spectra of substituted $Bi_xCo_{2-x}MnO_4$ contains three spectral features, A_2 (639 eV), B_2 (640.5 eV) and C_2 (642 eV), which can be directly compared with the three valence states (2+, 3+ and 4+) of Mn ions (see f gure 2). Spectra of the parent composition ($x = 0$) match well with those to the spectra of Mn^{3+} [19–21]. However, the increase in the intensity of peak features A_2 and C_2 with Bi substitution at the O_H site reveal that more of the Mn^{3+} ions are converted into Mn^{2+}/Mn^{4+}. The zoomed-normalized Mn L_3-edge region is shown as an inset in f gure 2, where increased Mn^{2+} and Mn^{4+} at the expense of Mn^{3+} is clearly displayed. Mn^{2+} occupies the T_D sites, complementing our observation of the reduced Co^{2+} in Co $L_{3,2}$ spectra, whereas Mn^{4+} ions are in O_H sites only, as the signature of Mn^{4+} is similar to MnO_2. The increase in Mn^{2+} and Mn^{4+} at the expense of Mn^{3+} results in the enhancement of net magnetic moment.

Figure 3 shows the measured O K-edge NEXAFS spectra of the $Bi_xCo_{2-x}MnO_4$, along with the spectra of reference compounds CoO, $LiCoO_2$, Bi_2O_3, MnO and MnO_2. O K-edge NEXAFS spectra, which represents the orbital nature of the spectral features of the O 2p unoccupied states in the conduction bands, can be eff ciently used to explore all kinds of possible hybridizations with different cations (Co, Mn and Bi). Based on the existing literature and band structure calculations [22–25], four spectral features marked by A_3-D_3 in $Bi_xCo_{2-x}MnO_4$ ($x = 0.1$) are identif ed. Except for the spectral feature B_3, all other features are present in the parent composition ($x = 0.0$). This is due to the reason

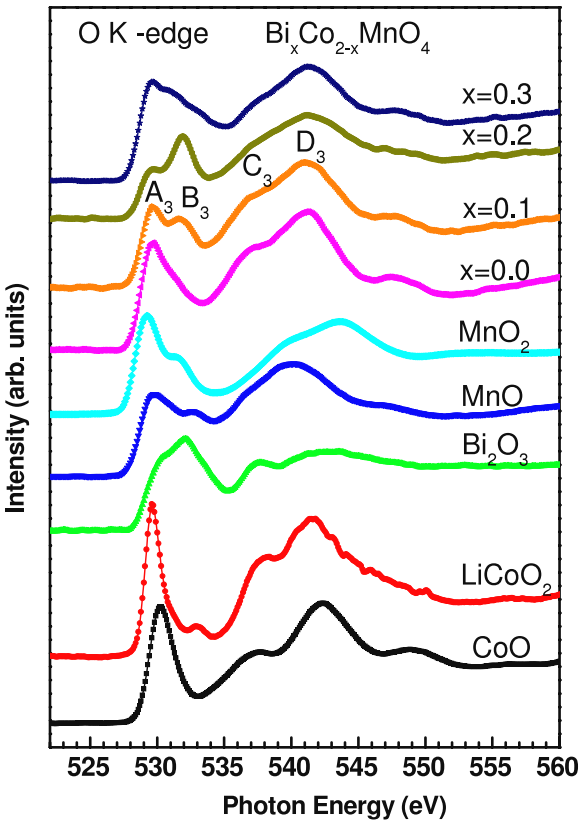

Figure 3. Normalized O K-edge spectra of $Bi_xCo_{2-x}MnO_4$ ($x = 0.0$, 0.1, 0.2 and 0.3) along with that of reference compounds CoO, $LiCoO_2$, MnO, MnO_2 and Bi_2O_3.

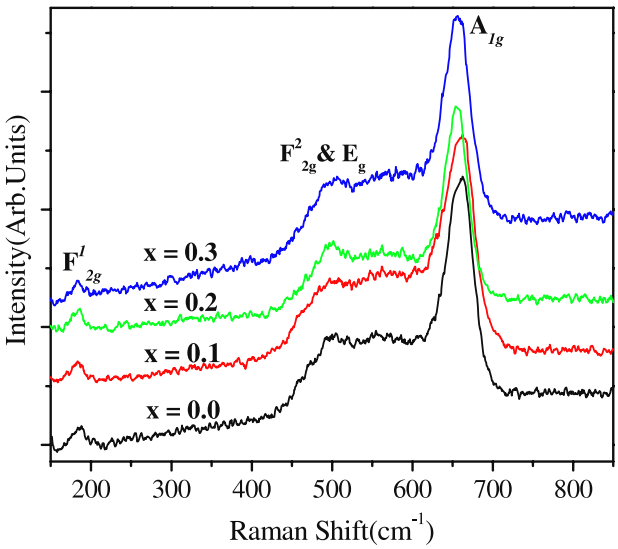

Figure 4. Raman scattering spectra collected at room temperature for $Bi_xCo_{2-x}MnO_4$ ($x = 0.0$, 0.1, 0.2 and 0.3).

that B_3 originates from Bi 6s/O 2p hybridizations. The O K-edge spectra of the pure ($x = 0.0$) sample indicates that low energy features resemble Co_3O_4 [26] and the spectral feature B_3 at ∼532 eV observed for doped compositions follows the behaviour of a highly polarizable $6s^2$ lone pair of electrons of the Bi^{3+} ion. The orientation of the Bi $6s^2$ lone pair towards a surrounding O^{2-} ion can produce local distortion and hybridization between the $6s^2$ Bi orbital and O 2p orbital, resulting in ferroelectric properties in doped compounds. As a matter of fact, increase of Bi content at the O_H site induces more Mn^{2+}/Mn^{4+} crystal symmetries, which can be clearly observed in the O K-edge spectra of an optimally doped ($x = 0.3$) sample, where A_3 is more prominent. On the whole, the spectral feature of peaks A_3, B_3, C_3 and D_3 clearly represents the presence of Bi^{3+}, $Mn^{2+/3+/4+}$ and $Co^{2+/3+}$ ions in Bi-substituted samples. The above observation is in conformity to the $L_{3,2}$ spectra of Co/Mn.

The element-specifi observation discussed above complements our structural measurement XRD [13] and Raman scattering. The parent compound, Co_3O_4, which crystallizes in the normal spinel structure with O_h^7 spectroscopic symmetry, was shown to possess f ve Raman-active modes, as $A_{1g} + E_g + 3F_{2g}$, with wavenumbers 194.4 cm^{-1} (F^1_{2g}), 482.4 cm^{-1} (E_g), 521.6 cm^{-1} (F^2_{2g}), 618.4 cm^{-1} (F^3_{2g}) and 691 cm^{-1} (A_{1g}) [27]. The Raman mode at ∼691 cm^{-1} (A_{1g}) is attributed to the characteristics of O_H sites (CoO_6) in the O_h^7 spectroscopic symmetry and the mode at ∼195 cm^{-1} (F^1_{2g}) is attributed to the T_D sites (CoO_4). The broadening and shifting of Raman modes on Mn substitution into the Co_3O_4 lattice is already reported [28]. Raman spectral studies of the $Bi_xCo_{2-x}MnO_4$ ($x = 0.0$, 0.1, 0.2 and 0.3) samples show a shift in peak positions towards lower wavenumbers (A_{1g} shifted from 664 to 650 cm^{-1} and F^1_{2g} shifted to 188–183 cm^{-1} for $x = 0.0$–0.3) due to increased unit cell parameters with Bi substitution (f gure 4). The greater shift in the A_{1g} mode indicates that the substituted Bi and most of the Mn cations are occupying the octahedral sites (Co/Bi/MnO_6). The shift in A_{1g} further indicates the domination of the octahedral environment, as Bi^{3+} ions with greater ionic radius occupy the octahedral sites. At the same time, the shift in the F^1_{2g} mode is not that more prominent, since the transition metal cations occupying the tetrahedral sites are of comparable radii. In general, the Raman spectra with a f at background are indicative of only a phonon structure present in the system, but the increased background at higher wavenumbers has been observed in large numbers of reports on superconductors [29] due to increased electronic scattering. $Bi_xCo_{2-x}MnO_4$ samples exhibited a considerable increase in the background at higher wavenumbers, which indicates that the multiferroic property of this material, which is strongly dependent on electron–phonon coupling, is evident at lower temperatures as well.

Regarding the magnetic behaviour of spinel oxides, there are mainly three types of magnetic interactions possible between the ions at A site and B sites through the intermediate oxygen ions (O^{2-}) via intrasite A–O–A (J_{AA}) and B–O–B ($J_{BB,}$), and intersite A–O–B (J_{AB}) superexchange interactions. In Co_2MnO_4 these interaction (J_{AA} and J_{BB}) energies are negative, favouring AFM. Simultaneously a positive, J_{AB}, superexchange interaction results in ferrimagnetism. In addition, with Bi substitution, a weak, J_{AA}, superexchange interaction between A sites (Co^{2+}–Co^{2+}) mediated through O^{2-} and Co^{3+} that maintains the AFM ordering is affected due to the redistribution of Co/Mn ions. The ferrimagnetic behaviour appears to evolve due to the Bi-substitution-

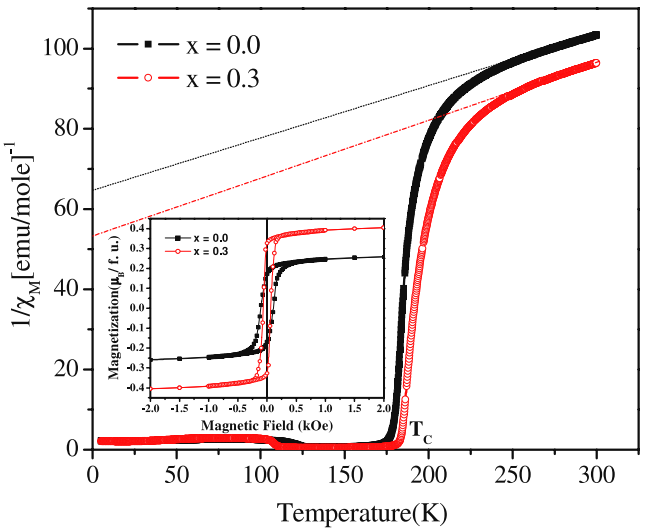

Figure 5. $1/\chi_M$–T plots $Bi_xCo_{2-x}MnO_4$ ($x = 0.0$ and 0.3). Inset: M–H loops $Bi_xCo_{2-x}MnO_4$ ($x = 0.0$ and 0.3) measured at 150 K.

induced competition among J_{AB} (Co^{2+}–O–Mn^{4+}, Co^{2+}–O–Mn^{3+}, Mn^{2+}–O–Mn^{3+}, Mn^{2+}–O–Mn^{4+}), J_{AA} (Co^{2+}–O–Co^{2+}, Mn^{2+}–O–Mn^{2+}, Co^{2+}–O–Mn^{2+}), J_{BB} (Mn^{3+}–O–Mn^{3+}, Mn^{4+}–O–Mn^{4+} and Mn^{3+}–O–Mn^{4+}) superexchange interactions and consequent magnetic frustration [14, 30]. The improvement in the ferrimagnetic property was confirmed through the rise in the ratio T_c/θ_{CW} [31], where θ_{CW} is the Curie–Weiss constant (which changes from 0.364 to 0.502 for $x = 0.0$–0.3 as observed from $1/\chi_M$ versus T plots, figure 5), which represents an increase in the frustration among the AFM ordering in the system, as Bi content increases. In other words, this can be interpreted by directly looking at the fall in negative Curie–Weiss constant, θ_{CW} (−494 to −370, for $x = 0.0$–0.3; obtained as the intersecting point of extrapolation of the high temperature region of $1/\chi_M$ versus T plots), which represent the fall in negative molecular field and consequent rise in AFM frustration, finally leading to improved ferrimagnetic behaviour. The increase in net magnetic moment because of the evolution of Mn^{2+} and Mn^{4+} (at the expense of Mn^{3+}) due to the Bi substitution is evident in M–H plots (inset of figure 5). However, it has to be mentioned that the well-defined ferrimagnetic behaviour exhibited by these compositions cannot be explained completely by the AFM frustration discussed so far. The canting of the spins by the Bi-induced structural distortion also contributes to ferrimagnetism. Therefore the source of increasing ferrimagnetic ordering with the Bi substitution in $Bi_xCo_{2-x}MnO_4$ ($0.0 \leqslant x \leqslant 0.3$) originates from the complex magnetic ordering attained and consequent enhancement in magnetic interactions. The NEXAFS study substantiates that the complex magnetic ordering is induced in the Bi-substituted spinel Co_2MnO_4.

4. Conclusions

In conclusion, we have investigated the electronic structure of $Bi_xCo_{2-x}MnO_4$ ($0.0 \leqslant x \leqslant 0.3$) using NEXAFS spectra at the O K edge and $L_{3,2}$ edge of Co/Mn. It has been shown that an increase in net magnetic moment and more ordered ferrimagnetism is due to Bi-induced cationic redistribution. More of the Mn^{3+} ions are converted into Mn^{2+} and Mn^{4+} and redistributed to T_D and O_H sites. Raman spectra of the samples confirm the greater occupation of substituted cations in the octahedral sites. A lowered negative molecular field is depicted by the decrease in Curie–Weiss constant, which indicates the increased AFM frustration with Bi substitution, supporting ferrimagnetic behaviour. O K edge spectra confirm the highly polarizable behaviour of the Bi $6s^2$ lone pair of electrons. Finally, Bi substitution introduces the radical change in cationic distribution and canting of the spins, favouring the ferrimagnetism along with the ferroelectricity.

Acknowledgments

The authors are grateful to Dr Amit Roy, Director IUAC, New Delhi for his keen interest and encouragement of this work, and DST, India for financial support under project no. SR/S2/CMP-0051/2007. One of the authors (NER) is grateful to IUAC, New Delhi, UGC, India, DCE and KSCSTE of State Government of Kerala and ZG College, Kerala, India for their support to carry out the research work. DKS acknowledges the financial support from CSIR, New Delhi, India. SKA and IVS are grateful to the Science Foundation of Ireland for financial support under project no. 06/IN.1/I91.

References

[1] Ramesh R and Spaldin N A 2007 *Nat. Mater.* **6** 21
[2] Bibes M and Barthelemy A 2008 *Nat. Mater.* **7** 425
[3] Pellier W, Singh M P and Murugavel P 2005 *J. Phys.: Condens. Matter* **17** R803
[4] Nan C-W, Bichurin M I, Dong S, Viehland D and Srinivasan G 2008 *J. Appl. Phys.* **103** 031101
[5] Yamasaki Y, Miyasaka S, Kaneko Y, He J P, Arima T and Tokura Y 2006 *Phys. Rev. Lett.* **96** 207204
[6] Akther Hossain A K M, Seki M, Kawai T and Tabata H 2004 *J. Appl. Phys.* **96** 1273
[7] Wolf S A, Awschalom D D, Buhrman R A, Daughton J M, von Molnár S, Roukes M L, Chtchelkanova A Y and Treger D M 2001 *Science* **294** 1488
[8] Carey M J, Maat S, Rice P, Farrow R F C, Marks R F, Kellock A, Nguyen P and Gumey B A 2002 *Appl. Phys. Lett.* **81** 1044
[9] Kahn M L and Zhang Z J 2001 *Appl. Phys. Lett.* **78** 3651
[10] Antic B, Goya G F, Rechenberg H R, Kusigerski V, Jovic N and Mitric M 2004 *J. Phys.: Condens. Matter* **16** 651
[11] Kumar S, Alimuddin, Kumar R, Dogra A, Reddy V R and Banerjee A 2006 *J. Appl. Phys.* **99** 08M910
[12] Ikedo Y, Sugiyama J, Nozaki H, Itahara H, Brewer J H, Ansaldo E J, Morris G D, Andreica D and Amato A 2007 *Phys. Rev.* B **75** 054424
[13] Rajeevan N E, Pradyumnan P P, Kumar R, Shukla D K, Kumar S, Singh A K, Patnaik S, Arora S K and Shvets I V 2008 *Appl. Phys. Lett.* **92** 102910
[14] Rajeevan N E, Kumar Ravi, Shukla D K, Pradyumnan P P, Arora S K and Shvets I V 2009 *Mater. Sci. Eng.* B **163** 48
[15] Lee H J, Kim G, Kim D H, Kang J-S, Zhang C L, Cheong S-W, Shim J H, Lee S, Lee H, Kim J-Y, Kim B H and Min B I 2008 *J. Phys.: Condens. Matter* **20** 295203
[16] de Groot F M F, Grioni M, Fuggle J C, Ghizsen J, Sawatzky G A and Petersen H 1989 *Phys. Rev.* B **40** 5715

[17] de Groot F M F, Fuggle J C, Thole B T and Sawatzky G A 1990 *Phys. Rev.* B **42** 5459
[18] van der Laan G and Kirkman I W 1992 *J. Phys.: Condens. Matter* **4** 4189
[19] Voss S, Fonin M and Rüdiger U 2007 *Phys. Rev.* B **75** 045102
[20] Mukherjee S and Pal A K 2006 *Phys. Rev.* B **74** 104413
[21] Harrison W A 2008 *Phys. Rev.* B **77** 245103
[22] Pellegrin E, Tjeng L H, de Groot F M F, Hesper R, Sawatzky G A, Moritomo Y and Tokura Y 1997 *J. Electron Spectrosc. Relat. Phenom.* **86** 115
[23] Park J H, Kimura T and Tokura Y 1998 *Phys. Rev.* B **58** R13330
[24] Dessau D S, Chuang Y D, Gromko A, Saitoh T, Kimura T and Tokura Y 2001 *J. Electron Spectrosc. Relat. Phenom.* **117/118** 265
[25] Hill N A and Rabe K M 1999 *Phys. Rev.* B **59** 8759
[26] van Elp J, L Wieland J, Eskes H, Kuiper P, Sawatzky G A, de Groot F M F and Turner T S 1991 *Phys. Rev.* B **44** 609
[27] Hadjiev V G, Iliev M N and Vergilov I V 1988 *J. Phys. C: Solid State Phys.* **21** L199
[28] Kovanda F and Rojka T 2006 *J. Solid State Chem.* **179** 812
[29] Iliev M N, Hadjiev V G, Jandl S, Le Boeuf D, Popov V N, Bonn D, Liang R and Hardy W N 2008 *Phys. Rev.* B **77** 174302
[30] Suzuki T, Nagai H, Nohara M and Takagi H 2007 *J. Phys.: Condens. Matter* **19** 145265
[31] Jeffrey Snyder G, Booth C H, Bridges F, Hiskes R, DiCarolis S, Beasley M R and Geballe T H 1997 *Phys. Rev.* B **55** 6453